1 **Smart Microdevices for Biomedical Drug Delivery: Endogenous Stimuli as**
2 **the Key to Safer Therapeutics**

3   Deepanjan Datta[1*], Viola Colaco[1], Maria Nison[2], Ananya Prabha H[1], Sony Priyanka Bandi[3],
4   Namdev Dhas[1], Vasudev R Pai[2], Praveen Halagali[1], Vamshi Krishna Tippavajhala[1],
5   Sudarshan Singh[4,5], Lalitkumar K. Vora[6]

6  [1]Department of Pharmaceutics, Manipal College of Pharmaceutical Sciences, Manipal
7  Academy of Higher Education, Manipal, India

8  [2]Department of Pharmacognosy, Manipal College of Pharmaceutical Sciences, Manipal
9  Academy of Higher Education, Manipal, India

10  [3]Department of Pharmacy, Birla Institute of Technology and Science (BITS) Pilani, Hyderabad
11  Campus, Hyderabad 500 078, Telangana State, India

12  [4]Faculty of Pharmacy, Chiang Mai University, Chiang Mai 50200, Thailand

13  [5]Office of Research Administration, Chiang Mai University, Chiang Mai 50200, Thailand

14  [6]School of Pharmacy, Queen's University Belfast, 97 Lisburn Road, Belfast BT9 7BL, UK

15  **\*Authors to whom correspondence is to be addressed**
16  Deepanjan Datta, PhD
17  Assistant Professor
18  Department of Pharmaceutics
19  Manipal College of Pharmaceutical Sciences
20  Manipal Academy of Higher Education, Manipal 576 104, Karnataka State, India
21  Email: deepanjan.datta@manipal.edu; deepanjandtt@gmail.com

### S4.1. Continuous liquid interface production (CLIP)

CLIP is a photopolymerization-based 3D printing technique that eliminates the recoating step by using an oxygen-permeable window to form a "dead zone", allowing continuous polymerization and rapid vertical layer construction at speeds up to 30 cm/h. Despite its speed and ability to reduce the staircase effect, it has limitations, including lower resolution (75 μm) and the need for lower-viscosity resins, restricting material choices [1–3].

### S4.2. Laser-induced forward transfer (LIFT)

LIFT is a precise material transfer technique using a pulsed laser to propel material from a donor ink layer to an acceptor substrate, enabling high-resolution patterning and 3D structure fabrication. The donor layer can be liquid, solid, or paste, allowing the use of various materials such as metal nanoparticles, hydrogels and biomaterials. LIFT offers resolution up to 10 μm and supports 2D/3D patterning. It has expanded to applications in sensors, capacitors, and bioprinting. Challenges include maintaining a minimal donor-to-acceptor distance and weak adhesion of transferred materials, limiting its use in microrobotics. Nonetheless, LIFT's broad material compatibility, high resolution, and versatility make it a promising tool for advanced technologies [4–6].

### S4.3. Inkjet printing (IJP)

IJP is a non-contact fabrication method that selectively deposits droplets (3-100 pL) onto substrates, allowing rapid evaporation to immobilize materials. It supports diverse inks, including piezoelectric, conductive, insulating, biocompatible, and enzyme-based formulations, making it adaptable for various applications. However, challenges like limited resolution (~50 μm), poor droplet placement control, and low interlayer adhesion restrict its utility for sub-10-micron precision tasks [4,5,7].

### S4.4. Stereolithography (SLA)

SLA is a foundational laser-based microfabrication technique that operates by utilizing a UV laser to cure a liquid monomeric resin into a solid structure. The process involves directing a laser beam at a tank containing photocurable liquid resin while a motorized stage facilitates vertical movement. The laser-induced cross-linking polymerization in the resin solidifies a predetermined pattern layer-by-layer. After fabrication, the unpolarized resin is removed

52 during a post-print development step [8,9]. Despite its high resolution (100 nm) and compatibility

53 with biodegradable resins, limitations in accuracy, material diversity, and fabrication speed

54 restrict its direct application in microrobot production [10]M. Valentin et al. demonstrated SLA

55 3D printing of alginate hydrogel using ionic crosslinking with divalent cations ($Ba^{2+}$, $Ca^{2+}$) to

56 achieve tunable degradation, mechanical properties, and pattern fidelity [11]. In another study by

57 Ziesmer and colleagues, they presented a method for fabricating photothermal MNs using a

58 low-cost SLA printer with plasmonic $Ag/SiO_2$ nanoaggregates in ultraviolet photocurable resin

59 [12]. The resulting MN arrays demonstrated sufficient mechanical strength, heating efficiency,

60 and the ability to increase intradermal temperature to clinically relevant levels under NIR

61 irradiation. The photothermal MNs showed effectively reduced bacterial growth in skin

62 infections and can be customized in size, shape, and needle geometry, offering promise in

63 treating bacterial skin infections (**Figure S1)**.
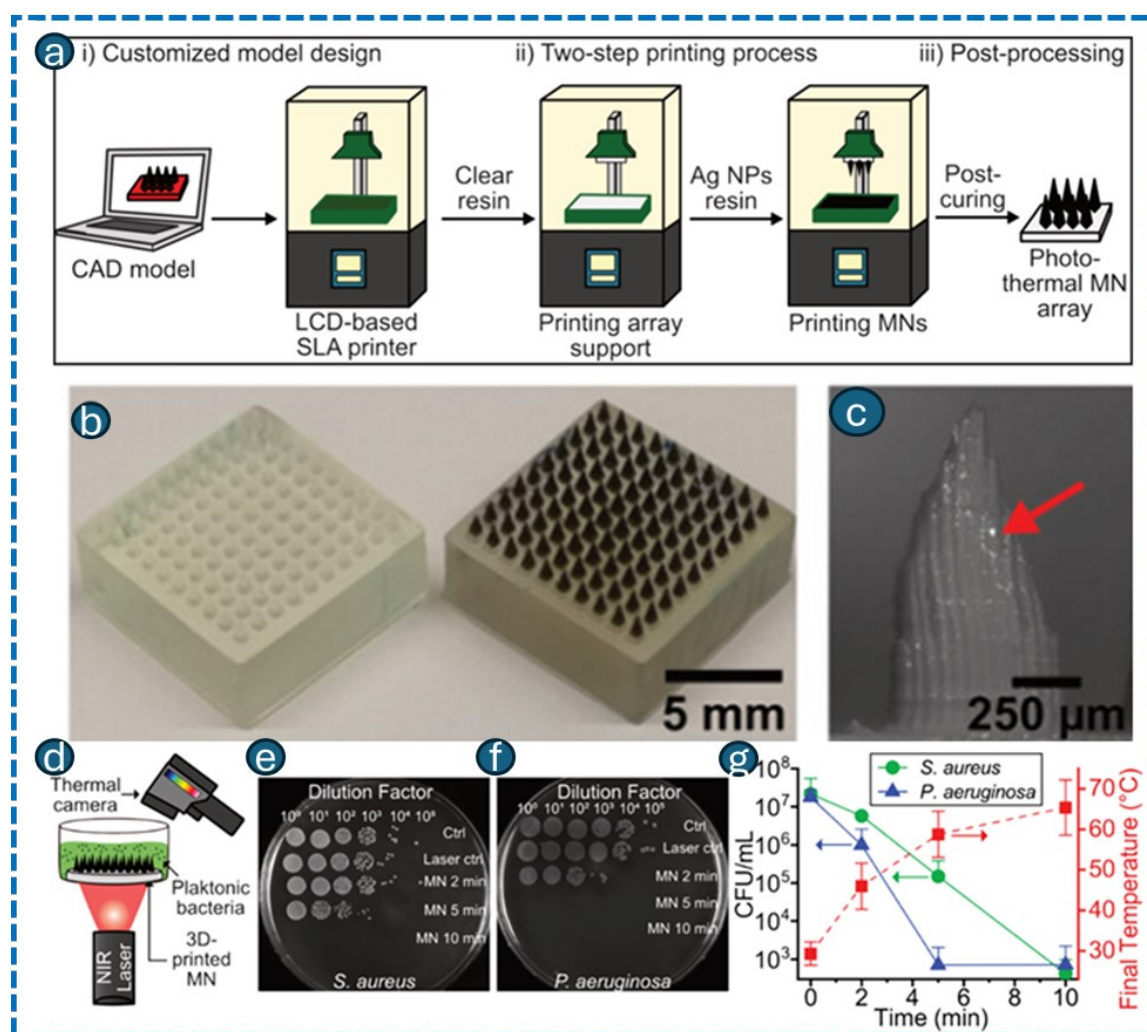


64 **Figure S1.** Schematic illustration of the two-step 3D printing process for photothermal

65 microneedle (MN) arrays: configuration of a customizable MN design onto an LCD-based SLA

66  printer (a.i), array support printing with clear UV resin and needles with plasmonic Ag/SiO$_2$ (2

67  wt% SiO$_2$) NP suspended in UV resin (a.ii), and post-curing in UV for 10 min (a.iii). Digital

68  images of different-shaped 3D-printed photothermal MN arrays with an Ag/SiO$_2$ NP-free MN

69  array (b). SEM image of a single photothermal MN indicating regions with silver-rich surface

70  (red arrow) (c). Antibacterial activity evaluation noted: schematic of the arrangement for

71  evaluation of temperature and antibacterial effects under 808 nm NIR irradiation (1 W cm$^{-2}$)

72  (d), agar plates showing serial dilutions of *S. aureus* (e) and *P. aeruginosa* (f) treated with MN

73  arrays at different time durations (0, 2, 5, 10 min), bacterial quantity (CFU mL$^{-1}$) of S. aureus

74  (green) and P. aeruginosa (blue) irradiated continuously along the final temperature profile

75  (red, n = 6) (g). The data are indicated as mean ± SD (n = 3). Reproduced from [12]. Copyright

76  2024, American Chemical Society.

77  **S4.5. Digital light processing (DLP)**

78  DLP is a photopolymerization-based microfabrication technique that rapidly creates 3D

79  structures by projecting UV light onto entire resin layers simultaneously. Unlike SLA, this

80  approach enhances printing speed and reduces oxygen interference. The limitations of DLP

81  include restricted choices of materials and a low-resolution range (25-100 μm) [12–14]. DLP has

82  been widely used in microfluidic devices [15] and allows the incorporation of functional

83  nanoparticles, such as carbon nanotubes, to enhance material properties [55]. A study by Wang

84  et al. developed poly(acrylic acid) (PAA)-based electroactive actuators fabricated using DL for

85  soft robotic applications [15]. The actuators respond to a low electric field (4-6 V), exhibiting

86  large deformation (43°), fast actuation (1.08 °/s), and stable performance. Enhanced actuation

87  was achieved with higher carboxyl group concentrations and thinner geometries, while high

88  cross-linking density increased mechanical strength and viscoelastic behaviour. A functional

89  membrane valve actuator was demonstrated, showcasing the potential of these tunable, cost-

90  effective materials for developing complex 3D-printed actuators for artificial muscles and soft

91  robotic systems. In another study, Gugulothu and Chatterjee introduced a cytocompatibility

92  bioink based on gelatin methacryloyl (GelMA) and poly(ethylene glycol) dimethacrylate

93  (PEGDM) for DLP-based 4D bioprinting using visible light (405 nm) photopolymerization

94  (Gugulothu and Chatterjee, 2023). The bioink enables hydration-induced shape morphing,

95  driven by differential cross-linking through photoabsorbers. The printed constructs mimic soft

96  tissue mechanics, support complex geometries, and maintain high cell viability and

97  proliferation, with NIH/3T3 cells attaining fibroblastic morphology. The findings position the

98 constructs as promising candidates for tissue engineering applications, including vascular

99 grafts, regeneration models and soft robotics **(Figure S2)**.
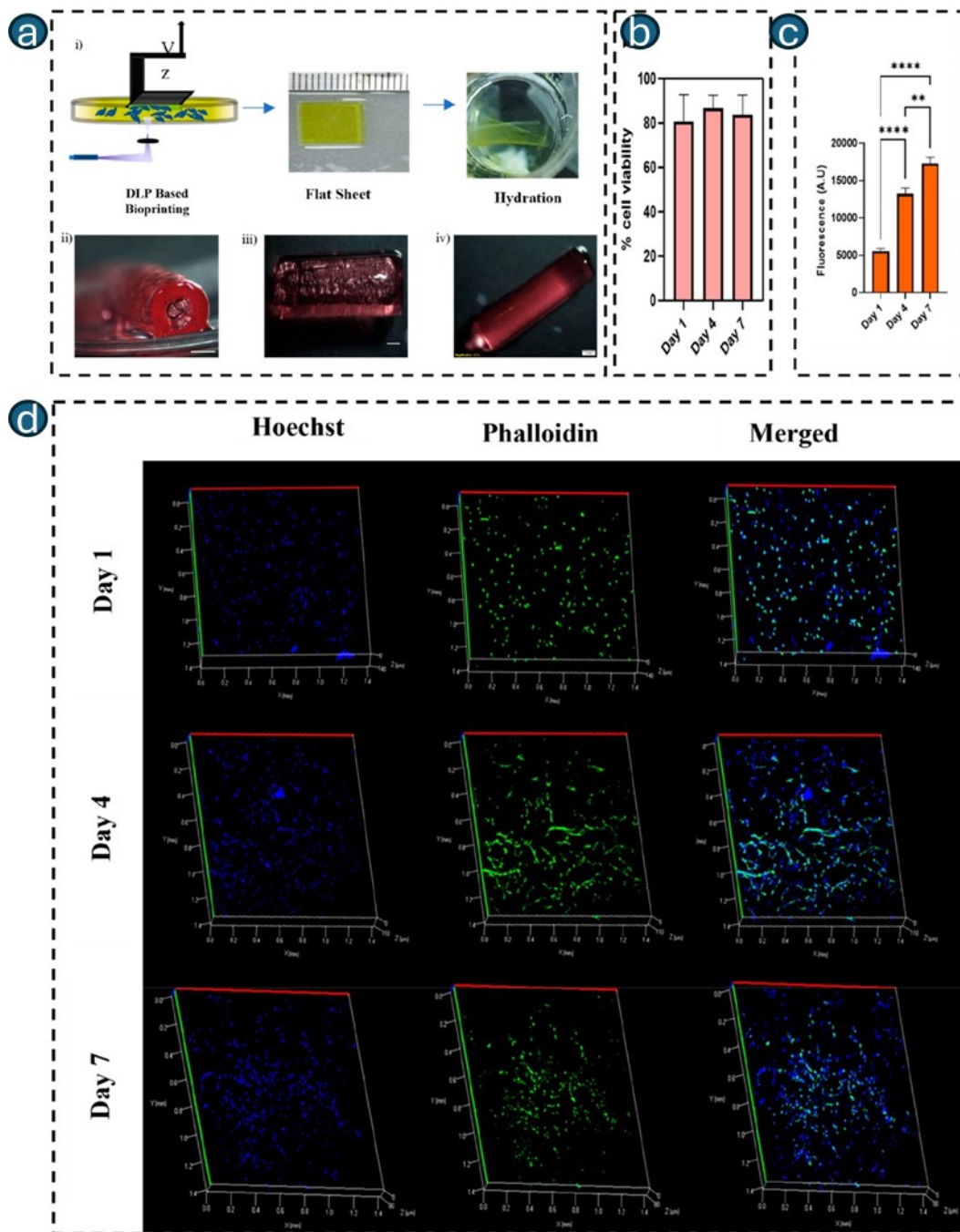


100 **Figure S2.** Biological characterization and Shape Deformability of 4D-Bioprinted Scaffolds:
101 Schematic representation of 3D bioprinting of a $10 \times 10 \times 0.8$ mm³ gel using P2.5G12.5 bioink
102 with NIH/3T3 cells (a. i), and shape transformation after 1-hour equilibration in media (scale
103 bar = 1 mm) (a.ii-iv). Metabolic activity of NIH/3T3 cells monitored over 7 days (b). The
104 percentage of living cells at various times was assessed via their Calcein AM (green) and
105 ethidium homodimer staining (c). 3D fluorescence imaging showing cytoskeleton (green) and

106 nucleus (blue), illustrating the morphological transition from spherical to fibroblastic shape (d).
107 Reproduced from [16]. Copyright 2023, American Chemical Society.

**S4.6. Two-photon polymerization (TPP)**

109 TPP, also known as direct laser writing (DLW), is a high-resolution 3D microfabrication
110 technique using an 800 nm femtosecond laser to induce nonlinear two-photon absorption in
111 photopolymer. This allows precise, localized polymerization at the laser's focal point, enabling
112 submicron resolution (<50 nm feature size and <150 nm lateral resolution) and exceptional
113 geometric flexibility [17,18]. TPP supports both additive and subtractive manufacturing and has
114 applications in microrobotics [19] and micro-electro-mechanical systems (MEMS) [20]. However,
115 challenges include slow fabrication speed, high costs, and limited structure height (<1mm).
116 Despite these, TPP shows promise in fields like drug delivery, cell manipulation, and
117 microsurgery, with ongoing efforts to enhance scalability and efficiency [5]. Isaakidou et al.
118 developed and characterized cochlear implants with anatomically relevant dimensions and
119 tunable microporous structures for localized drug delivery [21]. Using TPP with IP-Q resin,
120 implants with rectangular and cylindrical structures were fabricated, featuring precise pore
121 sizes (20 μm and 60 μm), partial hydrophilicity (contact angle: 72.3), and high polymerization
122 efficiency. The implants demonstrated excellent cytocompatibility, offering a novel approach
123 for targeted, personalized hearing loss treatment.

**S4.7. Selective laser sintering (SLS)**

125 SLS uses a laser to sinter fine powder particles below their melting point, fabricating 3D
126 structures layer-by-layer with isotropic mechanical properties. The technique involves three
127 key steps: powder deposition, laser-induced powder solidification, and vertical lowering of the
128 fabrication platform by one layer thickness. These steps are repeated iteratively to build the
129 desired 3D object [7,22,23]. Reusable powder particles enable 3D structures with 45 μm resolution.
130 SLS resolution depends on particle size, laser intensity, and scanning precision, with
131 conventional systems achieving 100-250 μm and advanced micro-SLS systems below 5 μm [6].
132 The limitations of the SLS technique include limited material options, high porosity, low
133 biocompatibility, rough surfaces, and elevated power and temperature requirements. Despite
134 limitations, SLS offers minimal anisotropy, complex structural fabrication, and reusable
135 support powders, showing potential for high-resolution microrobotics and biomedical
136 applications with ongoing advancements [4,7,24]. Mei and colleagues fabricated thermoplastic
137 polyamide elastomer (TAPE) film using SLS technology and demonstrated stable, repeatable,

138 and responsive behaviour for organic vapour sensing [25]. The microphase-separated structure

139 enabled vapour absorption, forming ionic pathways and reducing resistance, particularly for

140 polar solvents. These films also detected ethanol in breath monitoring, highlighting the

141 potential in wearable sensors and 4D printing.

## 142 **S4.8. Fused deposition modeling (FDM)**

143 FDM involves melting thermoplastic materials and extruding them through a nozzle to

144 fabricate 3D structures. It enables the cost-effective construction of complex shapes and allows

145 multi-material fabrication using multi-nozzle systems. FDM's limitations encompass reduced

146 resolution, elevated printing temperatures, limited material options, and a layer-by-layer finish

147 [4,26,27]. Lin et al. developed a 4D-printed, patient-specific, bioinspired absorbable left atrial

148 appendage occluder (LAAO) to address mechanical mismatches and biocompatibility issues of

149 traditional devices [28]. The actuator was composed of PLA and $Fe_3O_4$ nanoparticles. The

150 LAAO mimics LAA tissue mechanics using an optimized network design, offering tailored

151 geometry and a shape-memory transformation activated by minimally invasive magnetic field

152 implantation. The *in vivo* biocompatibility of sterilized 10PLA-MNC occluders was evaluated

153 by subcutaneous implantation in male Sprague-Dawley mice for 48 weeks. It demonstrated

154 excellent durability, biocompatibility after 48 weeks of implantation, and feasibility in

155 preclinical swine heart tests. Another study by Mousavi et al. presented a 3D-printed

156 multidirectional strain sensor for soft robotics [29]. Using a PLA-CNT composite, sensors and

157 conductive interconnects were directly printed with high sensitivity (gauge factor ~1342) and

158 selectivity (31.4x), enabled by a weak bond track design. Customization of sensitivity and

159 anisotropy is achieved by modifying air gaps, infill density, and build orientation. The sensors

160 can distinguish tensile and compressive bending, integrate seamlessly into soft robots, and

161 bypass the challenges of traditional mounting techniques. Despite low stretchability due to

162 material brittleness, placement near the axis mitigates this issue, paving the way for cost-

163 effective, multifunctional soft robotic systems.

## 164 **S4.9. Microextrusion 3D printing**

165 Microextrusion 3D printing constructs layer-by-layer structures with at least one dimension in

166 the micrometre range. The printable materials are extruded through a nozzle via mechanical,

167 electrical, or acoustic actuators, enabling continuous filament deposition. The advantages

168 include cost-effectiveness, solvent-free operation, high material viscosity compatibility, and

169 suitability for high cell density applications. However, it has limitations like cell damage during

170 printing, and restricted resolution hinders its application for finer structures [4,7]. Zhang et al.
171 developed a 3D-printed gelatin/bioceramics core/shell scaffold for treating an osteosarcoma-
172 related bone defect [30]. This study presented the development of 3D-printed scaffolds made of
173 bioceramics and gelatin, with doxorubicin (DOX)-loaded gelatin serving as the core and
174 SrCuSi4O10 (SC) nanosheets/beta-tricalcium phosphate ($\beta$-TCP) serving as the shell. SC
175 nanosheets provided photothermal treatment to the scaffolds when exposed to NIR-II laser
176 light. At the same time, the produced extreme heat might cause the gel-to-sol transition of the
177 gelatin in the filaments' central core, which in turn causes the loosening of the gelatin to release
178 DOX on demand, allowing for chemo-photothermal treatment. Synergistic anti-tumor effects
179 were shown by *in vitro* and *in vivo* studies demonstrating chemo-photothermal therapy **(Figure
180 S3)**. Furthermore, the scaffold's hollow channels were formed by the disintegration and release
181 of gelatin from the filaments, which served as visible architectural signals to encourage the
182 ingrowth of bone tissues. Degradation of SC nanosheets also helped to liberate bioactive ions
183 (Sr, Cu, and Si) over time, which boosted vascularized bone regeneration even more. These
184 findings pointed to the promising future of 3D-printed DOX-loaded gelatin-TCP/SC scaffolds
185 as a tool in the fight against osteosarcoma by destroying cancer cells and healing tumor-induced
186 bone deformities. Overall, the sequential treatment approach (anti-tumor therapy followed by
187 bone defect reconstruction), closely resembling the real clinical management of osteosarcoma
188 and aligned with the phased treatment protocols employed by orthopaedic surgeons, was
189 underscored in this study.
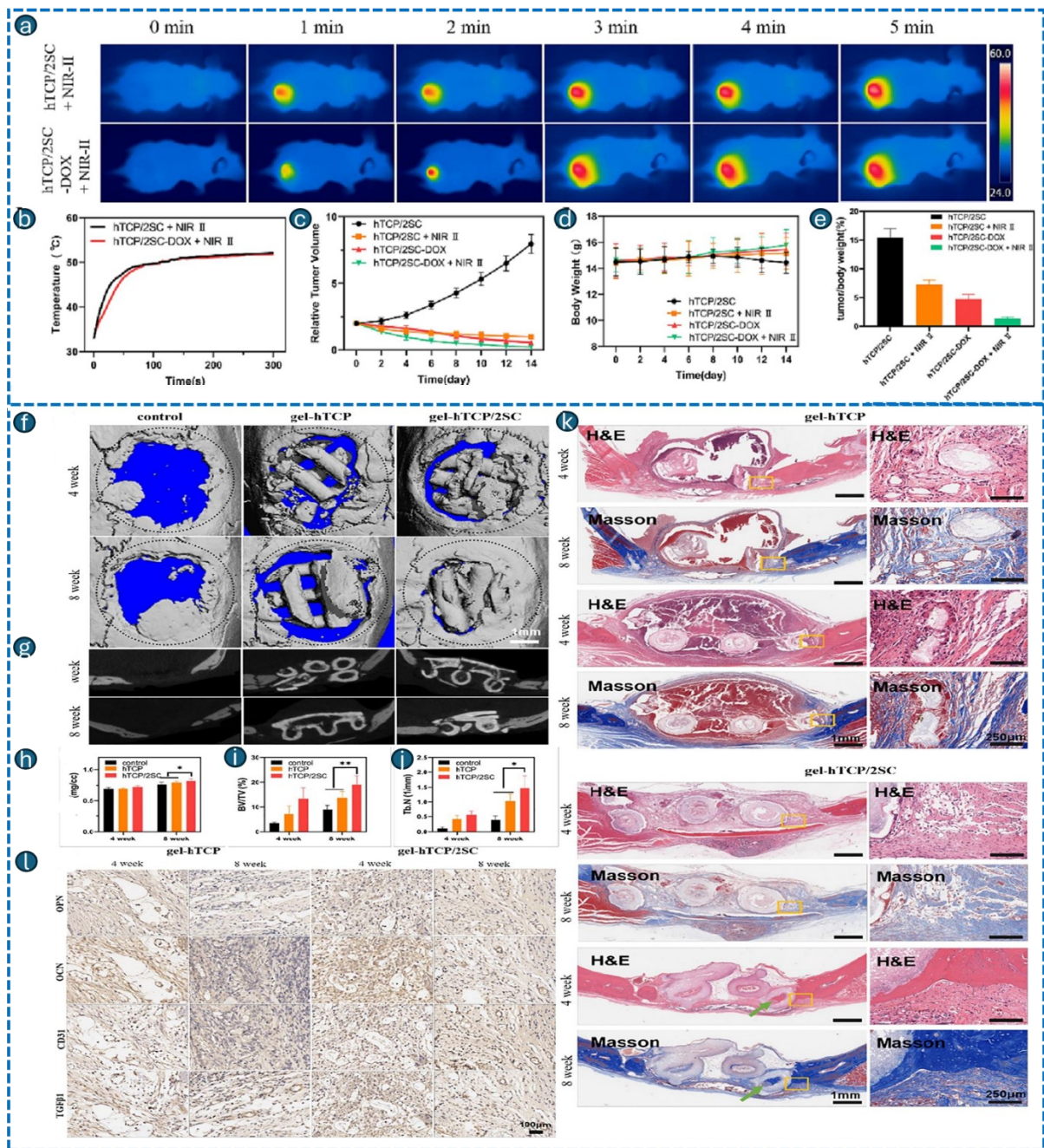
**Figure S3.** *In vivo* antitumor efficacy. Thermal images (a) and their corresponding photothermal heating curves (b) of *in vivo* 3D printed hTCP/2SC and hTCP/2SC-DOX composite scaffolds under 1064 nm laser irradiation (1.5 W/cm2, 5 min). Relative tumor volume (c), body weight (d), and tumor/body weight ratio (e) in mice after different treatments for 14 days. Evaluation of *in vivo* bone regeneration: 3D reconstruction of micro-CT images showing new bone formation in defect areas after different treatments for 4 and 8 weeks (f); and sectional views (g). Quantitative analysis of bone mineral density (BMD) (h), bone volume/tissue volume (BV/TV) (i), and trabecular bone number (Tb. N) (j) in the region of interest. H&E staining and Masson's trichrome staining of cranial defect sites after implantation

199  of 3D-printed gel-hTCP and gel-hTCP/2SC core/shell composite scaffolds for 4 and 8 weeks
200  (k). Immunohistochemical staining of newly formed tissues targeting OPN, OCN, CD31, and
201  TGFβ1 for treatment with gel-hTCP and gel-hTCP/2SC core/shell composite scaffolds for 4
202  and 8 weeks (l). Data expressed as mean ± SD (n = 5). Adapted with permission [30]. Copyright
203  2023, Elsevier.

204  Taken together, AM and 4D printing have very versatile and breakthrough technology in
205  crafting micro-devices owing to high control of complex geometries and multi-material
206  integration. Most notably, the development of such multi-stimuli-responsive systems augments
207  functionality both in biomedical and industrial applications, paving the pathways leading to
208  advanced innovations in precision medicine, soft robotics, and regenerative therapies. Research
209  and development of multi-purpose devices tailored to certain medical uses, such as
210  photothermal microneedles loaded with antimicrobial agents, gentle robotic sensors, and bio-
211  inks appropriate for tissue engineering. For instance, the incorporation of appropriate
212  functional materials, such as nanoparticles and stimulus-responsive polymers, makes them
213  exceedingly versatile in drug delivery approaches, cancer treatment, and regenerative
214  medicine. The continuous developments in material science and process optimization promise
215  a slew of innovative applications in health care and beyond.

216  **S5.1. Passive devices**

217  The principle of passive-delivery microdevices is the administration of a medication using
218  implant designs with one or more reservoirs. Reservoirs are hermetically sealed from the
219  delivery site by a polymeric membrane, which controls the activation and timing of release.
220  The substance of the membrane reacts chemically or biochemically with its surrounding
221  environment at the place of implantation to regulate the rate of membrane breakdown. Drugs
222  can be slowly and steadily released over an extended time using passive-delivery devices,
223  which rely on diffusion or osmotic pressure to transport the payload. Examples include the
224  fentanyl transdermal system (Duragesic) and the fluocinolone acetonide intravitreal implant
225  (Retisert), streamlining treatment delivery without integrated electronics. Because of the lack
226  of dose dependence and the fact that the medication distribution does not necessitate active
227  feedback control or telemetric activation, these devices are mostly reserved for the long-term,
228  continuous treatment of chronic conditions. The main benefits of this passive-delivery
229  microdevice type are its compact size, biocompatibility, huge payload capacity, ease of

230 operation, and ability to load a range of drug formulations. It also lacks the requirement for
231 supporting electronics [31].

232 At present, clinical applications make use of biodegradable polymers as passive-delivery
233 systems. After brain tumor removal, the residual tumor tissues can be treated with the
234 chemotherapeutic medication 1,3-bis(2-chloroethyl)-1-nitroso-urea (BCNU) (carmustine),
235 administered locally over three weeks using Gliadel polymer wafers [32]. The hydrolysis of the
236 biodegradable polymer causes the medication reservoirs in these delivery systems to gently
237 discharge their contents into the body. Controlled-release implantable devices can be
238 engineered from environmentally responsive hydrogels. Baldi et al. developed microvalves
239 made of double-sided structures with silicon membranes responsive to the stimulus of pH,
240 temperature, glucose concentration, etc., with higher response times than the existing systems.
241 These developed microvalves could be incorporated into autonomous systems that facilitate
242 reaction cycles inside microreaction chambers without the requirement of extra controlling
243 electronics [33]. Diabetes, exacerbated due to the rise of obesity rates, poses significant
244 challenges to global healthcare, especially due to poor adherence to insulin administration.
245 Glucose-responsive hydrogels present a promising avenue for controlled insulin delivery,
246 enhancing clinical reliability and effectiveness, while challenging researchers to refine
247 response kinetics and advance engineering of these systems. [34]. Passive resorbable millimetre-
248 sized devices constructed of compression-molded poly(l-lactic) acid (PLLA) reservoirs with
249 poly(lactide-co-glycolide) membranes were created by Grayson et al., as another form of
250 passive delivery device [35]. The medication was released over time as the multiple-reservoir
251 membranes broke down after implantation. Degradation of PLLA-based devices occurred
252 gradually over several months, enabling the release of medications and other biological
253 chemicals across the membrane prior to the complete absorption of the device at the implant
254 site. These molecules include heparin, human growth hormone, and dextran. Release via the
255 poly(lactide-co-glycolide) membranes occurred as water permeated the polymer, resulting in
256 swelling and hydrolysis. Polymers with higher molecular weights often require more time for
257 complete degradation, facilitating pulsatile and timely drug release through the incorporation
258 of various molecular weights in the membrane polymers.

259 To aggressively treat malignant gliomas, innovative passive-delivery devices were developed.
260 These devices have shown higher chemotherapeutic effectiveness of temozolomide compared
261 to BCNU (carmustine). The great efficacy of chemotherapeutic drugs like temozolomide, O6-
262 benzylguanine, and STAT3 inhibitor III in treating glioblastomas suggests their possible usage

with implantable drug-delivery systems. Future research on passive-delivery devices will explore methods for delivering multiple drugs simultaneously from multiple reservoirs, enhancing treatment efficacy for chronic illnesses requiring minimally invasive and localized drug delivery.

## S5.2. Active devices

These utilize numerous mechanisms for the controlled release of therapeutic agents, including micropumps driven by magnetic actuators, gas pressure, and electrothermal or electrochemical systems. These devices provide customized options for treating various diseases and can be either activated or deactivated after implantation. But these systems usually require miniature power electronics that increase the overall size of the system, which is mitigated by a telemetry system. Moreover, active devices provide precise control of the pharmacokinetic profile of drug delivery, unlike passive devices. The development of active-delivery devices using microelectrochemical systems (MEMS) technology was first intended for controlled-release applications. Early devices used electrochemical dissolution of gold or polymeric membranes to transport drugs to the site of action [36]. Pulsatile and regulated drug release from numerous reservoirs was possible with selective membrane activation. MEMS-based devices could precisely release several agents from a single device [37,38]. Li et al. subsequently showed *in vivo* delivery of the chemotherapeutic agent BCNU in rats using this technique [39].

### S5.2.1. Multifunctional MEMS devices

Multifunctional MEMS devices were developed for the simultaneous recording of neural activity and drug delivery. Altuna et al. prepared microprobes that are flexible by utilizing SU-8 polymer, incorporated electrodes made of platinum for sensing, and a microfluidic channel responsible for delivering the drug. Single-channelled probes like tetrodes and dual-channelled probes like linear probes were tested in live rats, and it was observed that these delivered therapeutic agents to brain-targeted areas, simultaneously recording neuronal activity, including spikes and ripples, demonstrating their flexibility in neuroscience research [40,41]. Despite decades of management of neurological diseases like Parkinson's and epilepsy with L-DOPA and anti-epileptic drugs, effective treatments remain elusive. Implantable devices such as neural stimulators arose as promising options; however, certain challenges, like poor biocompatibility leading to fibrosis and inflammation, need to be faced. A combination of drug delivery systems and neural probes using technologies like MEMS offers a potential solution

294   by providing simultaneous neural data recording as well as targeted drug delivery, addressing

295   symptoms as well as adverse effects [42,43].

296   **S5.2.2. Electrothermally actuated MEMS microchips**

297   Electrothermally actuated MEMS microchips are intriguing gadgets that utilize thermal

298   expansion to generate mechanical motion at the microscale. These are miniature mechanical

299   systems embedded within microchips. Actuation is accomplished using Joule heating, which

300   involves sending current through a microstructure to produce heat. Thermal expansion in

301   certain materials induced by heat leads to movement. Generally, it entails bimorph structures,

302   comprising two layers of materials with disparate thermal expansion coefficients. Upon

303   heating, one layer expands more significantly than the other, resulting in the structure bending

304   or twisting. Such a device was created for the intracranial delivery of drugs for the treatment

305   of malignant tumors in the brain [44]. This device employed an active MEMS approach to

306   improve drug release kinetics, potentially boosting efficacy and lowering toxicity. The

307   fundamental technique involved the melting of silicon nitride membranes through resistive

308   heating, facilitating a controlled drug release pattern, with each membrane providing a tailored

309   drug release configuration when activated individually.

310   Glioblastoma is considered a highly aggressive brain cancer form with low survival rates,

311   partially due to the challenges faced in drug delivery across the blood-brain barrier (BBB) [45].

312   The effectiveness of local implants remained limited, which were developed to bypass the

313   BBB; hence, an active microchip implant was developed, offering controlled drug delivery in

314   the brain [46]. However, refilling or a source of power exchange is not favourable for CNS

315   implants, as it involves risky procedures such as neurosurgery. This led to the development of

316   a MEMS device run electrothermally, showing its effectiveness *in vitro* as well as *in vivo* by

317   increasing the survival rates and controlling drug release in glioblastoma-induced rats.

318   Santini et al. developed an electrothermally actuated MEMS microchip that enables pulsative

319   and controlled release of chemicals from either multiple or single reservoirs [37]. A solid-state

320   silicon microchip may release one or more chemicals on demand. Thin anode membranes

321   covering microreservoirs packed with solid, liquid, or gel substances dissolve

322   electrochemically to release them. A prototype microchip using gold and saline solution as the

323   electrode material and release medium has shown regulated, pulsatile chemical release in

324   proof-of-principle release trials. Release studies showed that reservoir activation can be

325   modulated separately, enabling complicated release patterns. A gadget with a small size, fast

response times, and low power consumption may have other benefits. All chemical molecules to be released are stored in the microchip's reservoirs, enabling autonomous gadget development. Depending on the application, a microbattery, multiplexing circuitry, and memory could be integrated directly onto the device, allowing it to be mounted on a small probe, implanted, swallowed, integrated with microfluidic components to create a 'laboratory-on-a-chip,' or added to a standard electronic package. This innovation is followed by potential research showcasing the advancements of MEMS drug delivery systems in treating several ailments.

Postmenopausal women with low estrogen levels are at risk of osteoporosis, which is characterized by reduced bone density and degradation of bones, with a higher risk of fracture. A microchip device was developed that delivers parathyroid hormone, which stimulates the formation of bones. Human clinical trials performed on postmenopausal women confirmed the bioequivalence and safety of microchips to that of the standard subcutaneous delivery injections [47].

Massive blood loss and severe trauma often result in hemorrhagic shock, which needs immediate treatment to prevent death or any permanent damage. During limited healthcare facility access, hemostatic dressings are often self-applied, but they may not cure internal bleeding. Inotropic agents and vasopressin become crucial to managing this hemorrhagic shock. Hence, a biomedical microdevice was coined to treat hemorrhagic shock for emergency and ambulatory services, where this device treats high-risk patients by rapidly delivering vasopressin and holds the capability to address several acute conditions, such as neurological and cardiovascular emergencies [47]. A novel generation of drug-delivery devices has been developed expressly for trauma care, where swift intervention is essential for patient life. The implantable rapid-drug-delivery device (IRD[3]) was designed for the prompt treatment of hemorrhagic shock, utilizing vasopressin as a prototype medication [48]. The device was created as a prophylactic subcutaneous implant for high-risk individuals, such as troops in combat zones. The design includes a triggering algorithm that integrates blood pressure and heart rate data from conventional ECG and blood pressure sensors. It was comprised of a membrane, reservoir, and actuation layers. Microresistors present in the actuation layer produced heat by the passage of current, which induced the formation of bubbles and a rise in internal pressure, eventually rupturing the membrane and releasing the drug bolus swiftly.

**S5.2.3. Magnetically actuated MEMS drug delivery system**

[14]

358  A magnetically actuated MEMS drug delivery system was created to ensure regulated delivery
359  of chemotherapeutics. This device includes a magnetic membrane composite sealed
360  microreservoir. Membrane deflection is prompted by an external magnetic field, due to which
361  the internal pressure of the reservoir is increased, eventually facilitating diffusion of the drug
362  via micron-sized pores [49]. An anti-cancer drug, docetaxel, whose mechanism of action is the
363  disruption of the mitotic spindle, was selected to assess the device's release profile [50,51]. The
364  application of this device ranges from the treatment of various tumors, such as breast cancer,
365  emphasizing its necessity in local drug delivery and improved efficacy with minimal systemic
366  exposure. A freshly prepared docetaxel solution was compared *in vitro* with the drug released
367  through this device, and the results were matched, indicating the capability of utilising this drug
368  for clinical use, as well as further research and development.

369  **S5.2.4. Microfluidic hydraulic MEMS-based drug delivery devices**

370  Microfluidic hydraulic MEMS-based drug delivery devices run by stimulation via a
371  mechanism that was developed to deliver drugs within the inner ear using a microfluidic circuit
372  connected to microcannulas that enable the flow of fluid outside and inside the cochlea. The
373  compound dissolved within the fluid is delivered efficiently due to the rapid recharge and
374  discharge of fluid caused by different tubing sizes. This system offers a new pathway to its
375  utilization and study in clinical application, as it demonstrates an alteration in the action
376  potential threshold of the compound, providing effective penetration of drugs [52,53].
377  Sensorineural hearing loss is a condition that affects millions of people in the world. It
378  encompasses various conditions that affect the cochlea and vestibular parts of the inner ear,
379  caused by genetic mutations, infections, drug exposure, trauma, etc., eventually leading to
380  cochlear hair cell death. Cochlear implants provided various advancements in deafness
381  treatment; however, they lost efficacy due to the degeneration of cells. Novel devices such as
382  reciprocating micropumps showcase promising options to deliver treatment compounds
383  without affecting cochlear function and restoring perception to audio [54,55].

384  Taken together, to meet the growing demand for minimally invasive drug delivery methods,
385  innovative implantable biomedical microdevices have been developed through advancements
386  in MEMS and miniaturization technologies. These devices, both active and passive, can
387  administer precise doses of therapeutic agents at controlled intervals. The preceding sections
388  highlight the potential of these microdevices to enhance traditional approaches for managing
389  both acute and chronic conditions. With their highly engineered designs and capacity to tailor

390  individual pharmacokinetic profiles, they offer a unique platform for efficient, personalized

391  treatment with minimal invasiveness.

39 **Table S1.** Summary of stimuli-responsive microdevices and delivery systems categorized by trigger type, device format, and Technology Readiness Level 396 (TRL).

| Stimulus | Microdevice | Current TRL | Evidence supporting TRL | Translational Gap | Application | Ref. |
|---|---|---|---|---|---|---|
| Temperature | Disposable microfluidic Device (2015) | TRL 3–4 | Demonstrated controlled temperatures (37/42/50 °C, ±0.3 °C), increased apoptosis with MHIFU vs. incubation at 42 °C, and AFM-observed membrane *changes in vitro* studies | Lack of *in vivo* validation, HIFU-TSL dosing/thermometry & device scale-up pending | Model temperature-triggered chemotherapeutic release and cell-level effects | 56 |
| | Microparticle-based microdevice (2017) | TRL 2–3 | Supercritical fluid emulsion fabrication of magnetized PLGA/PLA microparticles is an established lab-scale method, surface coating enables tunable release, *in vitro* characterization typical for such systems; analogous microfluidic and microdevice platforms remain early-stage research tools | Lack of *in vivo* navigation validation studies | Targeted drug delivery with controlled release | 57 |
| | Soft microrobot (2018) | TRL 2–3 | Demonstrated *in vitro* with basic motion control and stimulus-responsive swelling, no evidence of animal validation | Complex navigation in *in vivo* studies, biocompatibility of long-term magnetic | Controlled local drug delivery (Proof-of-concept) | 58 |

[17]

| | | | | actuation, lack of scalable fabrication, and no preclinical safety studies | | |
|---|---|---|---|---|---|---|
| | Microfluidic hydrogel-based microcarriers (2018) | TRL 3 | Microfluidic fabrication and temperature-dependent release demonstrated *in vitro*, with no *in vivo* validation | Scaling microfluidic production, stability of thermo-responsive behaviour in physiological conditions, lack of biocompatibility and pharmacokinetic data | Controlled drug release, tunable thermos-responsive carrier system | 59 |
| | Actuators (2018) | TRL 2–3 | Demonstrated reversible hydrogel actuation, on-chip valve control, and tunable deformation in *in vitro* microfluidic prototypes, consistent with PNIPAM-based thermoresponsive device behaviour in microfabricated systems | Not intended for clinical use; poor long-term stability of thermogels, slow response time, challenges in scalability, sterilization, and integration with | Programmable microfluidic control, biomolecular handling, soft micro-robotics, lab-on-chip actuation | 60 |

| | | | | | | |
|---|---|---|---|---|---|---|
| | | | | biomedical workflows, no *in vivo* validation | | |
| | hMSC–microdevice complex (2019) | TRL 3 | Controlled and versatile attachment to hMSCs, complexes are stable after cultivation and trypsinization, no loss of proliferation, retained migration and spheroid behaviours in all *in vitro* studies | No *in vivo* validation, homing efficiency and biodistribution of hMSCs are known translational hurdles, need GMP-compliant microdevice fabrication and cell-product release testing; regulatory path for cell+device combination remains complex | Targeted/escort delivery using hMSCs while preserving motility and viability | 61 |
| | Microinjectors (2020) | TRL 3–4 | *In vitro* penetration through GI-mimicking hydrogels and *ex vivo* intestinal tissues, some prototypes tested in small animals, demonstrating successful mucosal insertion and | Requires safety validation for GI perforation risk, reproducible actuation timing, scalable | Oral delivery of biologics by trans-mucosal injection in the intestine | 62 |

| | | | localized drug release | microfabrication, biocompatible dissolution of components, and comprehensive *in vivo* pharmacokinetic studies prior to regulatory progression | | |
|---|---|---|---|---|---|---|
| | Microneedles (2022) | TRL 3–4 | Demonstrated microneedle mechanical insertion capacity, temperature-triggered swelling, and controlled drug release *in vitro*, some systems show *in vivo* animal pharmacodynamic enhancement and improved delivery efficiency | Need standardized mechanical robustness under physiological conditions, large-scale reproducibility, long-term stability of thermo-responsive polymers, safety validation for repeated skin application, and regulatory clarity for stimuli-responsive MNs | Controlled transdermal drug delivery | [63] |

[20]

| | | | | | | |
|---|---|---|---|---|---|---|
| | 3D-printed PNAGA hydrogel microrobot (2023) | TRL 3–4 | Demonstrated 3D printing feasibility, thermo-responsive drug release, and *in vitro* cytotoxicity, lack of *in vivo* tumour model testing | Complex *in vivo* navigation and targeting, long-term biocompatibility studies, limited understanding of tumor penetration, scalability and regulatory challenges for micro-robotic devices | Cancer therapy via temperature-triggered drug release | 64 |
| pH | Implantable pH-responsive drug-delivery device (2009) | TRL 3–4 | Extensive *in vitro* data and preclinical studies reported for pH-responsive hydrogels, implant design frameworks, modeling, and materials are well documented for implantable controlled release | Long-term biostability/degradation and mechanical robustness *in vivo* batch-consistent pH response, tissue–device integration, fouling, and sterilization; predictive in-human | Site-specific, on-demand release in acidic microenvironments, long-acting local therapy | 65 |

| | | | | release models, regulatory path for responsive implants vs. conventional long-acting depots | | |
|---|---|---|---|---|---|---|
| | Hydrogel-coated microcantilever sensing arrays (2011) | TRL 2–3 | Behaviour consistent with hydrogel-based microenvironment-responsive systems that demonstrate responsive swelling and biochemical sensitivity strictly *in vitro* without translational validation | No *in vivo* testing, challenges with hydrogel stability, cantilever drift, sterilization, long-term performance in physiological fluids, limited scalability, no regulatory pathway | Label-free detection of pH changes, analytes, and biochemical microenvironment cues, environmental/biomedical sensing | 66 |
| | Microspheres (2012) | TRL 3–4 | Fabrication of pH-responsive PLGA hollow microspheres, stable encapsulation of multiple drugs, MN mechanical strength sufficient for rat skin insertion, rapid dissolution of PVP MNs depositing HMNs, pH-triggered | Requires optimization for drug loading uniformity, long-term HM stability, and reproducibility of $CO_2$-triggered rupture | Smart transdermal multidrug delivery with two-stage, sequential release for combinational or staged therapy | 67 |

| | | | | | |
|---|---|---|---|---|---|
| | | | CO$_2$-mediated rupture causing controlled secondary drug release, and successful in-skin localization and diffusion of HMs | in more complex human skin pH environments. No large-animal or chronic-use safety studies, scaling PLGA HMN fabrication and MN integration under GMP is nontrivial. The regulatory pathway for multistage, reactive MNs systems remains undefined | |

| | Soft micro-robot (2016) | TRL 3–4 | Supports align with established fields: microfluidic drug-delivery devices enabling precise actuation and targeting, and pH-responsive hydrogels validated for controlled, environment-triggered drug release in preclinical contexts | Requires integration of magnetic actuation, hydrogel release, and biocompatible encapsulation. Challenges include *in vivo* navigation, immune clearance, biodegradation control, imaging guidance, and regulatory pathways for magnetically actuated implants | Site-specific delivery in tumor or inflamed acidic microenvironments | 68 |
|---|---|---|---|---|---|---|

| | | | | | |
|---|---|---|---|---|---|
| Microneedle (2018) | TRL 4 | Study shows show *in vivo* pharmacodynamics evaluation, greater anti-OVA IgG1 and CD8$^+$ T-cells vs soluble DNA vaccine and tumor rejection in B16/OVA melanoma; mechanism and composition detailed (OSM–(PEG-PAEU), poly(I:C), LbL MN coating) | Needs GMP-scalable MN manufacturing, sterilization, coating uniformity & shelf-life, human skin translation, dose-finding & safety; regulatory pathway for DNA vaccine + adjuvant on MN patches; broader clinical evidence for oncologic indications is pending | Cancer immunotherapy (DNA vaccine) via transcutaneous delivery with enhanced DC activation, type-I IFN, antibodies & CD8$^+$ T-cells | 69 |
| Microchannel-based system (2018) | TRL 3–4 | Geometric control of release rates, pH-responsive function verified with cell viability assays, all *in vitro* studies | Lacks the evidence of *in vivo* studies, needs biocompatibility studies and scale-up of microfabrication and regulatory path for channel-programmed, | Programmable multi-phase delivery of therapeutics in *in vitro* settings, foundational architecture for future implants | 70 |

[25]

| | | | | | | |
|---|---|---|---|---|---|---|
| | | | | multi-payload implants remain open | | |
| | Microrocket (2019) | TRL 4–5 | *In vivo* animal studies show enhanced local drug retention, magnetic targeting, and biodegradability of PASP/Fe–Zn components, supporting SI details zeta-potential, propulsion, and assay methods | Scale-up and manufacturability of uniform microrockets, navigation and imaging in complex gastric dynamics, long-term biocompatibility & by-product fate ($Zn^{2+}$/Fe species) in larger animals, regulatory path for self-propelled ingestible micromotors remains undefined | Targeted gastric delivery elevated mucosal retention | [71] |
| | Microneedle (2021) | TRL 3-4 | pH-responsive microneedle systems have been successfully demonstrated *in vivo* in animal models, showing | Requires validation in infection-bearing wound models, | Smart wound healing—on-demand release of | [72] |

| | | | microenvironment-responsive release, sustained therapeutic effects, and safe skin insertion. Evidence from analogous pH-responsive core-shell MNs shows environment-triggered rupture and prolonged drug action in rodent models | long-term safety of polymer coatings, and stability of pH-responsive performance in heterogeneous wound fluids, challenges in scaling uniform polymer coatings, sterility assurance, and regulatory classification as an adaptive wound-responsive medical device | antimicrobial/anti-inflammatory/analgesic agents in response to wound acidity, supports chronic wound management and skin-barrier repair | |
| --- | --- | --- | --- | --- | --- | --- |
| | Asymmetric microfluidic/chitosan pH-responsive device (2023) | TRL 3–4 | Demonstrated pH-dependent release and antibacterial performance *in vitro*, biocompatibility assessed, and initial *ex vivo* bone-mimetic testing | No *in vivo* bone defect validation, limited data on osteointegration, sterilization and mechanical robustness | Local drug release for infective bone defect treatment | 73 |

[27]

| | | | issues, manufacturing scalability, and regulatory challenges for implantable drug-release devices | | |
| Double-layered MOF-based micro swimmers (2024) | TRL 2–3 | *In vitro* propulsion, ROS-triggered dual-drug release, and cytotoxicity assays, no *in vivo* tumor studies | Poor propulsion in physiological conditions, potential metal toxicity, unclear clearance pathway, scale-up barriers, and regulatory uncertainty | Adaptive dual-drug anti-cancer therapy | 74 |

| | | | | | |
|---|---|---|---|---|---|
| Microneedle (2024) | TRL 4–5 | *In vivo* validation in rat postoperative pain model: MNs implant in skin within 15 min, pH-responsive shell rupture, prolonged ropivacaine release >72 h, significant reduction in mechanical & thermal pain sensitivity | Requires large-animal studies, long-term biocompatibility, and safety of microcrystal release kinetics; manufacturing scale-up of core–shell MNs, regulatory pathways for responsive MN analgesic systems not yet defined, need to validate self-monitoring accuracy across diverse wound types | Postoperative analgesia with >72 h sustained pain relief, responsive to incision microenvironment; minimally invasive local delivery | 75 |

| | | | | | |
|---|---|---|---|---|---|
| Enzyme | Shape-coded hydrogel microparticle-based multiplexed enzyme bioassay in a microfluidic device (2010) | TRL 2–3 | Demonstrated shape-coded hydrogel fabrication, enzyme immobilization, and simultaneous multi-analyte detection *in vitro*, compatible with microfluidic flow-based analysis; similar to other immobilized multi-enzyme microreactor systems used for analytical research | No clinical or *in vivo* relevance, enzyme stability limitations, mass-manufacturing of encoded particles, need for integration with validated clinical diagnostic workflows, and regulatory irrelevance for therapeutic translation | Multiplexed biochemical sensing, diagnostic assays, high-throughput screening | 76 |
| | Microfluidic device (2012) | TRL 2–3 | Demonstrated shape-coded hydrogel fabrication, enzyme immobilization, and simultaneous multi-analyte detection *in vitro*, compatible with microfluidic flow-based analysis; similar to other immobilized multi-enzyme microreactor systems used for analytical research | No clinical or *in vivo* relevance, enzyme stability limitations, mass-manufacturing of encoded particles, need for integration with validated clinical diagnostic workflows, and regulatory irrelevance for | Multiplexed biochemical sensing, diagnostic assays, high-throughput screening | 77 |

[30]

| | | | | | |
|---|---|---|---|---|---|
| | | | | therapeutic translation | |
| | Microneedles (2016) | TRL 4–5 | Demonstrated enhanced immune activation *in vitro* and *in vivo*, validated antitumor response with synergistic immunotherapy | Human skin penetration variability, dose-scaling for checkpoint inhibitors, safety and immune-related adverse event risk, GMP manufacturing of delivery system, regulatory hurdles for combination | Antitumor immunotherapy via transdermal delivery of checkpoint inhibitors | 78 |
| | Catalase-laden microdevice (2016) | TRL 3–4 | Demonstrated microdevice loading and stable attachment to cells, preserved cell viability, and enzyme activity *in vitro*, comparable systems show *in vivo* effects in rodents, supporting similar maturity levels | Needs controlled *in vivo* biodistribution, enzyme longevity, immunogenicity assessment, scalable fabrication, and regulatory definition for enzyme-device + living-cell | Antioxidant therapy, inflammation modulation, and cell-assisted enzyme delivery | 79 |

| | | | | | |
|---|---|---|---|---|---|
| | | | | combinational products | |
| | Actuator (2024) | TRL 3 | Demonstrated enzyme-triggered expansion, morphological change, and controlled release *in vitro*; no *in vivo* testing | Enzyme availability varies physiologically, with limited stability in complex biological fluids, scale-up of protein-PEGDA hybrid hydrogels, lack of biocompatibility and safety data for *in vivo* environments | Controlled drug release + shape-morphing hydrogel actuator | 80 |

| | | | | | | |
|---|---|---|---|---|---|---|
| | Microrobotic enzyme-responsive hydrogel delivery system (2025) | TRL 3–4 | Demonstrated targeted microrobotic navigation, enzyme-triggered drug release, and significant tumour suppression *in vitro* and *in vivo* studies | Challenges in deep-tissue microrobot navigation, enzyme variability between human tumours, long-term biocompatibility of microrobots, scale-up manufacturing, and complex regulatory pathway for combined micro-robotic therapeutic systems | Localized delivery of hydrogel-immobilized therapeutics for triple-negative breast cancer | 81 |
| Redox | Closed-loop drug-level control system (biosensor + controller + infusion pump) (2017) | TRL 5 | Demonstrated in live rabbits and rats: continuous measurement of doxorubicin levels and real-time dose adjustments; system maintained desired set-points despite inter-animal PK variability and acute drug–drug interactions | Requires miniaturization for human use, long-term biosensor stability, biocompatibility validation, clinical-grade pump integration, | Precision dosing of chemotherapeutics, patient-specific pharmacokinetic compensation | 82 |

| | | | cybersecurity/algorithm robustness, and a regulatory framework for automated closed-loop therapeutic systems | | |
|---|---|---|---|---|---|
| DNA-crosslinked, donor–acceptor (D–A) stimuli-responsive CMC hydrogels (2018) | TRL 2–3 | Reversible high/low stiffness via D–A or G-quadruplex switching, shape-memory & triggered self-healing demonstrated *in vitro* | Translation would require biostability in physiological fluids, enzymatic degradation control of DNA linkers, scalable synthesis & sterilization, and use-case/regulatory pathway definition | Smart functional hydrogel matrices for biosensing/actuation research | 83 |
| Miniaturized redox-capacitor assembled inside a microdevice (2018) | TRL 2-3 | Demonstrated selective assembly, surface functionalization, and electrochemical performance *in vitro*, supports toxin sensing and cell-response quantification in microfluidic environments, | Lack of *in vivo* studies requires enhanced stability, antifouling properties, high-throughput | Microbial toxin detection, mammalian cell cytotoxicity analysis, redox-based microfluidic bioassays | 84 |

| | | | comparable to other analytical microdevices such as spectro-electrochemical platforms and immobilized-enzyme microreactors | integration, standardized calibration, and no defined regulatory pathway for use beyond laboratory diagnostics | | |
|---|---|---|---|---|---|---|
| | Microneedle (2021) | TRL 4 | Demonstrated microneedle delivery, TME-triggered MIL-100(Fe) degradation, $O_2$ generation, and enhanced chemo-phototherapy *in vitro* and *in vivo* studies | Limited human skin penetration variability, uncertain Fe-based MOF metabolism/clearance, potential photothermal safety concerns, scale-up of MN-MOF integration, and regulatory barriers for combination nanomedicine-microneedle systems | $O_2$-evolving chemophototherapy for solid tumors | [85] |
| | Organohydrogel- | TRL 2–3 | 3D-stretchable devices (up to 500% | No *in vivo*/clinical | Stretchable | [86] |

| | based soft electronics with polyphenol-incorporated double networks (2022) | | strain), >1000 cycles at 200% strain with preserved performance, >200 mF·cm$^{-2}$ capacitance; multi-component (TA/EG) gels enabling robust interfaces, all demonstrated *in vitro*/lab-scale prototypes | data, long-term biocompatibility and sweat/skin environment stability; sterilization and packaging, large-area manufacturing and device encapsulation, regulatory path for wearable bioelectronic materials remains to be defined | bioelectronics for wearable/skin-like devices | |
|---|---|---|---|---|---|---|

| | | | | | |
|---|---|---|---|---|---|
| | Wireless bioelectronic device (2024) | TRL 4–5 | Demonstrated controlled electrochemical release, wireless programmability, and significant tumour suppression *in vivo* studies | Long-term biocompatibility of implanted electronics, risk of electrochemical byproducts, complex regulatory path for active implantable, manufacturing scalability, and human-scale intratumoral dosing challenges | Localized, programmable intratumoral drug release for breast cancer | 87 |
| | 4D-printed redox-responsive needle panel meter (2025) | TRL 2–3 | Demonstrated programmable 4D-printed geometric deformation under redox conditions; validated glucose and lactate sensing *in vitro* studies, lack of biological or clinical validation | Lacks the long-term clinical validation, requires manual enzymatic steps, needs microfluidic integration, sample preprocessing required, | Quantitative sensing of glucose and lactate concentrations | 88 |

[37]

| | | | | lab-optimized conditions are unlikely to translate directly to field use, no continuous wear/biocompatibility data, and not benchmarked against clinical CGM standards | | |
|---|---|---|---|---|---|---|
| | 3D-printed spectro-electrochemical platform for redox-based bioelectronic device (2025) | TRL 2–3 | Demonstrated 3D-printed microdevice fabrication, integrated electrode–optical detection, and redox signal characterization *in vitro*, typical of spectro-electrochemical microdevices designed for analytical testing | Not clinically oriented, requires improved sensitivity, electrode stability, biofouling resistance, standardized calibration, and integration with validated clinical | Biosensing, redox-based biochemical analysis, lab-on-chip bioelectronics | 89 |

| | | | | diagnostic workflows | | |
|---|---|---|---|---|---|---|
| Hypoxia | Microfluidic device generating tunable oxygen gradients (2015) | TRL 3 | Similar hypoxia-engineered platforms demonstrate controlled oxygen gradients and 3D hypoxic microenvironments for studying cancer and endothelial cell responses *in vitro* and *in vivo* | No *in vivo* validation; microdevice does not replicate full tumor microenvironment (ECM, immune cells, perfusion); challenges in scaling for drug-screening pipelines, regulatory irrelevance for therapeutic development | *In vitro* evaluation of hypoxia-dependent cytotoxicity of anticancer drugs, cancer microenvironment modeling | 90 |
| | Microdevice platform recapitulating hypoxic tumor microenvironments (2017) | TRL 2–3 | Demonstrated formation of physiologically relevant oxygen gradients, validated with oxygen sensor imaging, numerical modeling, and spatially resolved hypoxic signaling in cancer cells, entirely *in vitro* prototype research | Not intended for *in vivo* use, lacks physiological complexity, challenges in scaling, standardization, and integration with | *In vitro* modeling of tumor hypoxia, signaling studies, gradient mapping, and drug-response assays | 91 |

| | | | | regulated diagnostic workflows, and regulatory path irrelevant to clinical therapeutics because it is an analytical research tool | | |
| --- | --- | --- | --- | --- | --- | --- |
| | $O_2$-controllable laccase-crosslinked gelatin hydrogel (2017) | TRL 4 | Platform validated through polymer synthesis, $O_2$-monitoring assays, rheology, and 3D cell encapsulation, shown to control hypoxia gradients in standard culture and rodent *in vivo* systems | Requires biostability optimization for long-term implantation; limited by host-immune response, diffusion-limited nutrient transport, scalability for therapeutic use, and no regulatory pathway | Studying hypoxia-driven cell behaviour *in vitro*, evaluating tissue grafts & tumor models *in vivo* | 92 |

[40]

| | High-throughput microfluidic system with linear oxygen gradient (2021) | TRL 3–4 | Demonstrated high-throughput spheroid generation and exposure to five distinct oxygen levels: quantified ROS and drug responses (doxorubicin, tirapazamine) in breast tumor spheroids *in vitro* | Not suitable for *in vivo* use, limited to *in vitro* modelling, device fabrication complexity, integration challenges for clinical workflows, and no regulatory pathway since it is a research-only microfluidic platform | Study of chronic/cyclic hypoxia, ROS generation, and drug cytotoxicity in tumor spheroids | 93 |
|---|---|---|---|---|---|---|
| | Oxygen-tunable endothelialized microvascular chip (2025) | TRL 3–4 | Demonstrated precise control of oxygen levels over endothelialized microchannels, enabling hypoxia–reperfusion cycles *in vitro*, consistent with other validated microfluidic oxygen-control systems used for tumor and disease modeling | Limited to *in vitro* disease modelling, lacks systemic circulation, immune components, and hemodynamic complexity, and fabrication challenges for large-scale use | Modeling hypoxia–reperfusion injury and vaso-occlusion in sickle cell disease | 94 |
| Ionic | Salt-responsive | TRL 2–3 | Demonstrated reversible salt-induced | Not validated in | Antifouling coatings, | 95 |

| | | | swelling, lubrication switching, and reduced protein/cell adsorption *in vitro,* consistent with known zwitterionic brush behaviour and responsive polymer-surface engineering literature | complex biological environments; long-term stability under physiological ionic strengths unresolved, scale-up and substrate-compatibility challenges; regulatory pathway undefined | tunable-friction surfaces, biosensing and marine/medical surface protection | |
|---|---|---|---|---|---|---|
| | zwitterionic polymer brushes (2015) | | | | | |
| | Hydrogel (2017) | TRL 3–4 | Analogous multi-stimuli hydrogels demonstrate *in vitro* responsiveness and occasional rodent-model validation of microenvironment-triggered behaviour, supporting similar developmental maturity | No standardized *in vivo* pharmacokinetics, enzymatic response varies across tissues; need for GMP-grade polypeptide synthesis; mechanical stability and sterilization challenges; regulatory uncertainty for multi- | Site-specific drug delivery in pathological microenvironments with simultaneous ionic/pH/enzymatic cues | 96 |

| | | | | trigger, biodegradable peptide hydrogels | | |
|---|---|---|---|---|---|---|
| | Degradable soft ionic microdevices (2020) | TRL 2–3 | Demonstrated stretchability, ionic conductivity, rapid self-healing, and controlled degradation *in vitro*, device prototypes and basic electromechanical performance shown in lab conditions | No *in vivo* validation, long-term biocompatibility and degradation-product safety unknown; challenges in sterilization, integration with electronics, and scaling of organohydrogel fabrication, unclear regulatory pathway for degradable soft-ionic implantable | Soft bioelectronics, wearable/implantable sensing, soft robotic microdevices | 97 |
| | Zwitterionic polymer-brush (2020) | TRL 2–3 | Demonstrated synthetic grafting of zwitterionic brushes onto hydrogel matrices, ion-responsive friction | No validation under physiological shear/ionic | Low-friction, antifouling, and tunable-lubrication | 98 |

| | | | coefficients measured *in vitro*, behaviour consistent with other zwitterionic salt-responsive polymer brush studies | complexity, long-term stability in biological fluids uncertain; scaling of brush-hydrogel grafting, no regulatory framework | hydrogel coatings, biomaterial surface engineering | |
| --- | --- | --- | --- | --- | --- | --- |
| | Microneedles (2023) | TRL 4–5 | Fabrication by template replication + 3D transfer printing, ion-tunable mechanics demonstrated, *in vivo* efficacy in diabetic rat full-thickness wounds with enhanced healing/regeneration | Need GMP-grade exosomes and batch consistency, long-term safety of indwelling tips, sterilization & shelf-life, human-skin adhesion/retention variability, combo-product regulatory path (device + biologic) | Diabetic ulcer healing (pro-angiogenic, immunomodulatory exosome delivery) | 99 |
| | Agar/alginate wet-spun microfiber-shaped | TRL 2-3 | Typical agar/alginate wet-spun microfibers show controllable mechanical behaviour, ionic responsiveness, and | No stability/safety data under physiological pH, | Soft actuators, micro-scaffolds, and responsive microfiber | 100 |

| | | | | | |
|---|---|---|---|---|---|
| | hydrogel (2023) | | microscale patterning, used strictly *in vitro* as functional hydrogel materials | complex degradation behaviour, need for reproducible micro-topographic manufacturing, no regulatory framework, and a lack of *in vivo* studies | platforms for sensing or cell-guidance | |
| | Ionic-liquid–mediated organogel for Cyclosporine A transdermal delivery (2024) | TRL 4–5 | Comparable hydrogel and organogel systems have been validated *in vitro* and *in vivo* in rodent models, demonstrating controlled microenvironment-responsive behaviour and effective delivery under physiological conditions | Requires long-term dermal toxicity studies, variability of ionic liquid safety across species, need for human skin permeation validation, organogel scalability and stability, and regulatory ambiguity for ionic-liquids enhanced pharmaceutical | Topical treatment of psoriasis via localized Cyclosporine A delivery without systemic toxicity | 101 |

| | | | | | |
|---|---|---|---|---|---|
| | | | formulations | | |
| Microgels (2025) | TRL 2–3 | Demonstrated ion-triggered crosslinking, tunable rheology, printability, and shape-changing behaviour *in vitro* studies, similar to other early-stage microfluidic and oxygen-controlled biofabrication platforms, used only in lab environments | No biological validation; long-term stability unknown, scaling issues for manufacturing, lack of biocompatibility testing *in vivo*, unclear regulatory pathway for printed smart materials | 3D and 4D (bio)printing for dynamic constructs, shape-morphing materials | 102 |

394 **TRL 1, 2:** Basic principles observed, technology concept formulated**; TRL 3:** Experimental proof of concept shown in lab**; TRL 4:** Laboratory validation of 395 component/process**; TRL 5:** Validation in relevant biological models**; TRL 6:** Prototype demonstration in preclinical/ GLP studies**; TRL 7:** Prototype 396 demonstration in human clinical trials Phase I**; TRL 8:** Technology qualified and approval (regulatory clearance)**; TRL 9:** Actual system proven in routine 397 clinical/ market use

## References

1   B. J. Lee, K. Hsiao, G. Lipkowitz, T. Samuelsen, L. Tate and J. M. DeSimone, *Addit. Manuf.*, 2022, **55**, 102800.

2   C. T. Hagan, C. Bloomquist, I. Kim, N. M. Knape, J. D. Byrne, L. Tu, K. Wagner, S. Mecham, J. DeSimone and A. Z. Wang, *Acta Biomater.*, 2022, **148**, 163–170.

3   R. Janusziewicz, J. R. Tumbleston, A. L. Quintanilla, S. J. Mecham and J. M. DeSimone, *Proceedings of the National Academy of Sciences*, 2016, **113**, 11703–11708.

4   S. R. Dabbagh, M. R. Sarabi, M. T. Birtek, S. Seyfi, M. Sitti and S. Tasoglu, *Nat. Commun.*, 2022, **13**, 1–24.

5   F. M. den Hoed, M. Carlotti, S. Palagi, P. Raffa and V. Mattoli, *Micromachines 2024, Vol. 15, Page 275*, 2024, **15**, 275.

6   A. Das, A. Ghosh, S. Chattopadhyaya and C. F. Ding, *Opt. Laser Technol.*, 2024, **168**, 109893.

7   J. Li and M. Pumera, *Chem. Soc. Rev.*, 2021, **50**, 2794–2838.

8   I. Xenikakis, M. Tzimtzimis, K. Tsongas, D. Andreadis, E. Demiri, D. Tzetzis and D. G. Fatouros, *European Journal of Pharmaceutical Sciences*, 2019, **137**, 104976.

9   F. P. W. Melchels, J. Feijen and D. W. Grijpma, *Biomaterials*, 2010, **31**, 6121–6130.

10  T. D. Ngo, A. Kashani, G. Imbalzano, K. T. Q. Nguyen and D. Hui, *Compos. B Eng.*, 2018, **143**, 172–196.

11  T. M. Valentin, S. E. Leggett, P. Y. Chen, J. K. Sodhi, L. H. Stephens, H. D. McClintock, J. Y. Sim and I. Y. Wong, *Lab Chip*, 2017, **17**, 3474–3488.

12  J. Ziesmer, I. Sondén, J. Venckute Larsson, P. Merkl and G. A. Sotiriou, *ACS Appl. Bio Mater.*, 2024, **7**, 4533–4541.

13  X. Wang, J. Liu, Y. Zhang, P. M. Kristiansen, A. Islam, M. Gilchrist and N. Zhang, *Virtual Phys. Prototyp.*, DOI:10.1080/17452759.2023.2248101.

14  I. Ertugrul, *Micromachines 2020, Vol. 11, Page 518*, 2020, **11**, 518.

15  Z. Luo, H. Zhang, R. Chen, H. Li, F. Cheng, L. Zhang, J. Liu, T. Kong, Y. Zhang and H. Wang, *Microsyst. Nanoeng.*, 2023, **9**, 1–13.

16  S. B. Gugulothu and K. Chatterjee, *ACS Macro Lett.*, 2023, **12**, 494–502.

17  M. Carlotti, O. Tricinci and V. Mattoli, *Adv. Mater. Technol.*, 2022, **7**, 2101590.

18  W. Wang, Z. Q. Chen, B. Lin, M. C. Liu, Y. Zhang, S. J. Liu, Y. Li and Q. Zhao, *Chemical Engineering Journal*, 2024, **493**, 152469.

19  T. Zandrini, S. Taniguchi and S. Maruo, *Micromachines 2017, Vol. 8, Page 35*, 2017, **8**, 35.

20  S. Pagliano, D. E. Marschner, D. Maillard, N. Ehrmann, G. Stemme, S. Braun, L. G. Villanueva and F. Niklaus, *Microsyst. Nanoeng.*, 2022, **8**, 105.

21  A. Isaakidou, I. Apachitei, L. E. Fratila-Apachitei and A. A. Zadpoor, *Journal of Functional Biomaterials 2023, Vol. 14, Page 494*, 2023, **14**, 494.

436 22   E. O. Olakanmi, R. F. Cochrane and K. W. Dalgarno, *Prog. Mater. Sci.*, 2015, **74**, 401–
437        477.

438 23   P. Kulinowski, P. Malczewski, E. Pesta, M. Łaszcz, A. Mendyk, S. Polak and P.
439        Dorożyński, *Addit. Manuf.*, 2021, **38**, 101761.

440 24   S. R. Dabbagh, M. R. Sarabi, R. Rahbarghazi, E. Sokullu, A. K. Yetisen and S. Tasoglu,
441        *iScience*, 2021, **24**, 102012.

442 25   S. Mei, Z. Li, X. Chen, W. Zhao, Y. Zhang, X. Zhang, Z. Cui, P. Fu, X. Pang and M. Liu,
443        *Journal of Materials Research and Technology*, 2023, **26**, 5095–5104.

444 26   S. C. Ligon, R. Liska, J. Stampfl, M. Gurr and R. Mülhaupt, *Chem. Rev.*, 2017, **117**,
445        10212–10290.

446 27   M. O. F. Emon, F. Alkadi, D. G. Philip, D. H. Kim, K. C. Lee and J. W. Choi, *Addit.
447        Manuf.*, 2019, **28**, 629–638.

448 28   C. Lin, L. Liu, Y. Liu and J. Leng, *ACS Appl. Mater. Interfaces*, 2021, **13**, 12668–12678.

449 29   S. Mousavi, D. Howard, F. Zhang, J. Leng and C. H. Wang, *ACS Appl. Mater.
450        Interfaces*, 2020, **12**, 15631–15643.

451 30   X. Zhang, H. Wei, C. Dong, J. Wang, T. Zhang, L. Huang, D. Ni and Y. Luo, *Chemical
452        Engineering Journal*, 2023, **461**, 141855.

453 31   N. M. Elman, Y. Patta, A. W. Scott, B. Masi, H. L. Ho Duc and M. J. Cima, *Clin.
454        Pharmacol. Ther.*, 2009, **85**, 544–547.

455 32   M. A. Moses, H. Brem and R. Langer, *Cancer Cell*, 2003, **4**, 337–341.

456 33   A. Baldi, M. Lei, Y. Gu, R. A. Siegel and B. Ziaie, *Sens. Actuators B Chem.*, 2006, **114**,
457        9–18.

458 34   E. Ginter and V. Simko, *Adv. Exp. Med. Biol.*, 2013, **771**, 42–50.

459 35   A. C. Richards Grayson, I. S. Choi, B. M. Tyler, P. P. Wang, H. Brem, M. J. Cima and R.
460        Langer, *Nat. Mater.*, 2003, **2**, 767–772.

461 36   Where a Pill Won't Reach on JSTOR, https://www.jstor.org/stable/26060243, (accessed
462        25 October 2025).

463 37   J. T. Santini, M. J. Cima and R. Langer, *Nature*, 1999, **397**, 335–338.

464 38   F. Frankel, DOI:10.1002/1521-3773(20000717)39:14.

465 39   Y. Li, R. S. Shawgo, B. Tyler, P. T. Henderson, J. S. Vogel, A. Rosenberg, P. B. Storm,
466        R. Langer, H. Brem and M. J. Cima, *Journal of Controlled Release*, 2004, **100**, 211–219.

467 40   A. Altuna, E. Bellistri, E. Cid, P. Aivar, B. Gal, J. Berganzo, G. Gabriel, A. Guimerà, R.
468        Villa, L. J. Fernández{ Ef and L. Menendez De La Prida{, 2013, **13**, 1422.

469 41   K. Gao, G. Li, L. Liao, J. Cheng, J. Zhao and Y. Xu, *Sens. Actuators A Phys.*, 2013, **197**,
470        9–14.

471 42   Y. Zhong and R. V. Bellamkonda, *Brain Res.*, 2007, **1148**, 15–27.

472 43   S. T. Retterer, K. L. Smith, C. S. Bjornsson, K. B. Neeves, A. J. H. Spence, J. N. Turner,
473        W. Shain and M. S. Isaacson, *IEEE Trans. Biomed. Eng.*, 2004, **51**, 2063–2073.

474 44    B. C. Masi, B. M. Tyler, H. Bow, R. T. Wicks, Y. Xue, H. Brem, R. Langer and M. J.
475       Cima, *Biomaterials*, 2012, **33**, 5768–5775.

476 45    G. alias R. R. Naik, R. S. P, S. R. Jadhav, R. Pokale, P. Hedayat, D. Datta, B. Prajapati,
477       S. Mutalik and N. Dhas, *ACS Pharmacol. Transl. Sci.*, 2025, **2025**, 3410.

478 46    Panigrahi M, D. Pk and P. Pm, *Indian J. Cancer*, DOI:10.4103/0019-509X.76623.

479 47    R. Farra, N. F. Sheppard, L. McCabe, R. M. Neer, J. M. Anderson, J. T. Santini, M. J.
480       Cima and R. Langer, *Sci. Transl. Med.*, DOI:10.1126/SCITRANSLMED.3003276.

481 48    N. M. Elman, H. L. Ho Duc and M. J. Cima, *Biomed. Microdevices*, 2009, **11**, 625–631.

482 49    F. N. Pirmoradi, J. Jackson, H. Burt and M. Chiao, *2011 16th International Solid-State
483       Sensors, Actuators and Microsystems Conference, TRANSDUCERS'11*, 2011, 2831–
484       2834.

485 50    J. B. Wolinsky, Y. L. Colson and M. W. Grinstaff, *Journal of Controlled Release*, 2012,
486       **159**, 14–26.

487 51    S. Alken and C. M. Kelly, *Cancer Manag. Res.*, 2013, **5**, 357–365.

488 52    E. E. L. Pararas, D. A. Borkholder and J. T. Borenstein, *Adv. Drug Deliv. Rev.*, 2012, **64**,
489       1650–1660.

490 53    J. Fiering, M. J. Mescher, E. E. Leary Swan, M. E. Holmboe, B. A. Murphy, Z. Chen, M.
491       Peppi, W. F. Sewell, M. J. McKenna, S. G. Kujawa and J. T. Borenstein, *Biomed.
492       Microdevices*, 2009, **11**, 571–578.

493 54    Otology          &          Neurotology,          https://journals.lww.com/otology-
494       neurotology/citation/1985/03000/Cochlear_Implants__1981_To_1985.13.aspx,
495       (accessed 25 October 2025).

496 55    C. L. Budenz, B. E. Pfingst and Y. Raphael, *The Anatomical Record: Advances in
497       Integrative Anatomy and Evolutionary Biology*, 2012, **295**, 1896–1908.

498 56    L. Meng, Z. Deng, L. Niu, F. Li, F. Yan, J. Wu, F. Cai and H. Zheng, *Theranostics*, 2015,
499       **5**, 1203–1213.

500 57    V. Cricchio, M. Best, E. Reverchon, N. Maffulli, G. Phillips, M. Santin and G. Della
501       Porta, *J. Pharm. Sci.*, 2017, **106**, 2097–2105.

502 58    H. Lee, H. Choi, M. Lee and S. Park, *Biomed. Microdevices*, DOI:10.1007/s10544-018-
503       0344-y.

504 59    Y. H. Roh, J. Y. Moon, E. J. Hong, H. U. Kim, M. S. Shim and K. W. Bong, *Colloids
505       Surf. B Biointerfaces*, 2018, **172**, 380–386.

506 60    L. D'eramo, B. Chollet, M. Leman, E. Martwong, M. Li, H. Geisler, J. Dupire, M.
507       Kerdraon, C. Vergne, F. Monti, Y. Tran and P. Tabeling, *Microsystems &
508       Nanoengineering 2018 4:1*, 2018, **4**, 17069-.

509 61    J. Xia, A. C. Tsai, W. Cheng, X. Yuan, T. Ma and J. Guan, *Biomater. Sci.*, 2019, **7**, 2348–
510       2357.

511 62    A. Ghosh, L. Li, L. Xu, R. P. Dash, N. Gupta, J. Lam, Q. Jin, V. Akshintala, G. Pahapale,
512       W. Liu, A. Sarkar, R. Rais, D. H. Gracias and F. M. Selaru, *Sci. Adv.*, 2020, **6**, 4133–
513       4161.

63    J. Y. Li, Y. H. Feng, Y. T. He, L. F. Hu, L. Liang, Z. Q. Zhao, B. Z. Chen and X. D. Guo, *Acta Biomater.*, 2022, **153**, 308–319.

64    Y. Zhou, M. Ye, H. Zhao and X. Wang, *Int. J. Bioprint.*, 2023, **9**, 709.

65    J. Chen, M. Chu, K. Koulajian, X. Y. Wu, A. Giacca and Y. Sun, *TRANSDUCERS 2009 - 15th International Conference on Solid-State Sensors, Actuators and Microsystems*, 2009, 1465–1468.

66    D. S. Vanblarcom and N. A. Peppas, *Biomedical Microdevices 2011 13:5*, 2011, **13**, 829–836.

67    C. J. Ke, Y. J. Lin, Y. C. Hu, W. L. Chiang, K. J. Chen, W. C. Yang, H. L. Liu, C. C. Fu and H. W. Sung, *Biomaterials*, 2012, **33**, 5156–5165.

68    H. Li, G. Go, S. Y. Ko, J. O. Park and S. Park, *Smart Mater. Struct.*, 2016, **25**, 027001.

69    H. T. T. Duong, Y. Yin, T. Thambi, T. L. Nguyen, V. H. Giang Phan, M. S. Lee, J. E. Lee, J. Kim, J. H. Jeong and D. S. Lee, *Biomaterials*, 2018, **185**, 13–24.

70    D. Yang, J. S. Lee, C. K. Choi, H. P. Lee, S. W. Cho and W. H. Ryu, *Acta Biomater.*, 2018, **68**, 249–260.

71    M. Zhou, T. Hou, J. Li, S. Yu, Z. Xu, M. Yin, J. Wang and X. Wang, *ACS Nano*, 2019, **13**, 1324–1332.

72    A. Ullah, M. Jang, H. Khan, H. J. Choi, S. An, D. Kim, Y. R. Kim, U. K. Kim and G. M. Kim, *Sensors and Actuators B-chemical*, DOI:10.1016/j.snb.2021.130441.

73    H. Chen, W. Tan, T. Tong, X. Shi, S. Ma and G. Zhu, *Int. J. Mol. Sci.*, DOI:10.3390/ijms24054616.

74    Y. Zhong, H. Li, T. Jiang, X. Mu, M. Seki and U. K. Cheang, *Advanced Intelligent Systems*, 2024, **6**, 2400244.

75    A. Zhang, Y. Zeng, B. Xiong, X. Jiang, Y. Jin, S. Wang, Y. Yuan, W. Li and M. Peng, *Adv. Funct. Mater.*, 2024, **34**, 2314048.

76    E. Jang and W. G. Koh, *Sens. Actuators B Chem.*, 2010, **143**, 681–688.

77    M. K. L. Chu, J. Chen, C. R. Gordijo, S. Chiang, A. Ivovic, K. Koulajian, A. Giacca, X. Y. Wu and Y. Sun, *Lab Chip*, 2012, **12**, 2533–2539.

78    Y. Ye, J. Wang, Q. Hu, G. M. Hochu, H. Xin, C. Wang and Z. Gu, *ACS Nano*, 2016, **10**, 8956–8963.

79    J. Xia, Z. Wang, Y. Yan, Z. Cheng, L. Sun, Y. Li, Y. Ren and J. Guan, *Langmuir*, 2016, **32**, 13386–13393.

80    Y. Liu and L. R. Khoury, *Small science*, DOI:10.1002/smsc.202400214.

81    M. Tian, M. Keshavarz, A. A. Demircali, B. Han and G. Z. Yang, *Small*, DOI:10.1002/smll.202408813.

82    P. L. Mage, B. S. Ferguson, D. Maliniak, K. L. Ploense, T. E. Kippin and H. T. Soh, *Nature Biomedical Engineering 2017 1:5*, 2017, **1**, 0070-.

551 83 C. Wang, M. Fadeev, M. Vázquez-González and I. Willner, *Adv. Funct. Mater.*, 2018,
552 **28**, 1803111.

553 84 W. Shang, Y. Liu, E. Kim, C. Y. Tsao, G. F. Payne and W. E. Bentley, *Lab Chip*, 2018,
554 **18**, 3578–3587.

555 85 S. Luo, Y. Zhao, K. Pan, Y. Zhou, G. Quan, X. Wen, X. Pan and C. Wu, *Biomater. Sci.*,
556 2021, **9**, 6772–6786.

557 86 W. Wang, F. Chen, L. Fang, Z. Li and Z. Xie, *ACS Appl. Mater. Interfaces*, 2022, **14**,
558 12583–12595.

559 87 M. Souri, S. Elahi and M. Soltani, *Expert Opin. Drug Deliv.*, 2024, **21**, 495–511.

560 88 T. H. Yang, Y. S. Birhan, P. C. Chu, L. R. Chanu and P. S. Lai, *Mater. Des.*,
561 DOI:10.1016/j.matdes.2025.114228.

562 89 C. Y. Chen, E. Kim, F. R. Zakaria, M. J. Chu, B. Wu, G. F. Payne and W. E. Bentley,
563 *Small Methods*, 2025, **9**, 2401843.

564 90 Z. Wang, Z. Liu, L. Li and Q. Liang, *Microfluidics and Nanofluidics 2015 19:6*, 2015,
565 **19**, 1271–1279.

566 91 Y. Ando, H. P. Ta, D. P. Yen, S. S. Lee, S. Raola and K. Shen, *Scientific Reports 2017
567 7:1*, 2017, **7**, 15233-.

568 92 D. M. Lewis, M. R. Blatchley, K. M. Park and S. Gerecht, *Nature Protocols 2017 12:8*,
569 2017, **12**, 1620–1638.

570 93 R. Primavera, M. Razavi, B. D. Kevadiya, Y. Zhang, F. Jiang, Y. Charles Zhao, al -, S.
571 Flores-Torres, O. Peza-Chavez, H. Kuasne, I. Berger Fridman, G. Stefano Ugolini, V.
572 VanDelinder, S. Cohen and T. Konry, *Biofabrication*, 2021, **13**, 035037.

573 94 S. R. Schad, J. D. Beckman, W. A. Lam and D. K. Wood, *Lab Chip*, 2025, **25**, 4920–
574 4933.

575 95 J. Yang, H. Chen, S. Xiao, M. Shen, F. Chen, P. Fan, M. Zhong and J. Zheng, *Langmuir*,
576 2015, **31**, 9125–9133.

577 96 G. Ma, W. Lin, Z. Yuan, J. Wu, H. Qian, L. Xu and S. Chen, *J. Mater. Chem. B*, 2017, **5**,
578 935–943.

579 97 L. Fang, J. Zhang, W. Wang, Y. Zhang, F. Chen, J. Zhou, F. Chen, R. Li, X. Zhou and Z.
580 Xie, *ACS Appl. Mater. Interfaces*, 2020, **12**, 56393–56402.

581 98 A. O. Osaheni, A. Ash-Shakoor, I. Gitsov, P. T. Mather and M. M. Blum, *Langmuir*,
582 2020, **36**, 3932–3940.

583 99 X. Zhang, J. Gan, L. Fan, Z. Luo and Y. Zhao, *Advanced Materials*, 2023, **35**, 2210903.

584 100 W. Yekai, L. Haoran, Y. Kun, L. Xiufang, L. Zhentan and W. Dong, *Carbohydr. Polym.*

585 101 D. Datta, S. P. Bandi and V. V. K. Venuganti, *ACS Omega*, 2024, **9**, 41565–41582.

586 102 V. Pal, D. Gupta, S. Liu, I. Namli, S. H. A. Rizvi, Y. O. Yilmaz, L. Haugh, E. M. Gerhard
587 and I. T. Ozbolat, *Small*, 2025, **21**, e02262.